NUCL SCI TECH (2016) 27:76
DOI 10.1007/s41365-016-0073-y

A review of geometric calibration for different 3-D X-ray imaging systems

Yao Yang[1,2] · Liang Li[1,2] · Zhi-Qiang Chen[1,2]

Received: 8 April 2015 / Revised: 25 May 2015 / Accepted: 1 June 2015 / Published online: 18 May 2016

Abstract A precise knowledge of geometry is always pivotal to a 3-D X-ray imaging system, such as computed tomography (CT), digital X-ray tomosynthesis, and computed laminography. To get an accurate and reliable reconstruction image, exact knowledge of geometry is indispensable. Nowadays, geometric calibration has become a necessary step after completing CT system installation. Various geometric calibration methods have been reported with the fast development of 3-D X-ray imaging techniques. In these methods, different measuring methods, calibration phantoms or markers, and calculation algorithms were involved with their respective advantages and disadvantages. This paper reviews the history and current state of geometric calibration methods for different 3-D X-ray imaging systems. Various calibration algorithms are presented and summarized, followed by our discussion and outlook.

Keywords 3-D X-ray imaging system · Computed tomography · Geometric calibration · Reconstruction

This work was supported by the National Natural Science Foundation of China (No. 81427803 and 61571256) and the Beijing Excellent Talents Training Foundation (No. 2013D009004000004).

✉ Liang Li
lliang@tsinghua.edu.cn

1 Department of Engineering Physics, Tsinghua University, Beijing 100084, China

2 Key Laboratory of Particle and Radiation Imaging (Tsinghua University), Ministry of Education, Beijing 100084, China

1 Introduction

The importance of geometric calibration cannot be underestimated. In a typical 3-D X-ray imaging system, computed tomography (CT), for example, the X-ray tube, assumes different discrete positions along a trajectory. For each source position, a projection image (a radiograph) is acquired [1]. Reconstruction of the imaged object is accomplished by the imaging system. In the last few decades, a large number of reconstruction algorithms have been published devote to improving the image quality, which includes some famous algorithms like FDK, Grangeat's algorithm, Katsevich's algorithm, and back-projection filtration (BPF) algorithm. However, the image quality promotions are limited by the lack of a precise knowledge of the system geometry. 3-D X-ray system geometry refers to the relative positions of the X-ray focal spots and the location of the digital detector. A precise calibration of the system geometry can overcome problems, such as the blurring effect and artifacts, and becomes the most important factor for a better reconstructed image.

The development of geometric calibration was a substantial improvement to computer imaging. We can easily obtain a high image quality and a high level of detail resolution of a reconstructed structure in the imaged object with calibrated system geometry. Various calibration methods have been employed in medical or industrial imaging, which have already achieved good results in practical applications. This paper will summarize the current state of geometry calibration in different 3-D X-ray imaging systems. Also, a brief history of geometric calibration will be given, followed by a description of various methods. As these methods are suitable for different 3-D X-ray imaging systems, we will introduce them with a classification according to the systems where they are employed.

2 Background

In order to get a relatively accurate system geometry, various calibration methods have been reported. Due to some technical limitations, most of them were carried out within the past two decades.

Early methods determined the system geometry by physically measuring the spatial location of the different components. Although these methods can get a relatively accurate geometry, they require a number of precise measurements and are typically complex. After early methods, researchers proposed a series of mathematical methods which employ some point-like markers and calibrate the system geometry with the markers' trajectory on the detector plane. These methods can calibrate the system geometry with just several simple materials. However, they cannot calibrate the entire geometrical parameters and they are only suitable to some general scanning trajectory, such as cone beam CT or spiral CT. Besides, some calibration methods were also developed for the imaging system, which has a specific scanning trajectory, such as tomosynthesis, computed laminography, and limited-angle CT [2–4]. While these systems may not have a conventional scanning mode, some markers and their locations in the projected image were used to determine the relative positions between the components of the system. Last but not least, methods with a well-designed phantom also existed. Although these methods can acquire an accurate geometry, the phantoms used were always very expensive and were not convenient for practical applications. Nowadays, more and more practical methods have been introduced for geometric calibration. These methods may determine the system geometry with only some simple point-like markers located at any position within the imaged space and can obtain relatively accurate system geometry when dealing with practical applications.

In conclusion, we cannot get a reconstructed image of a high quality without an exact knowledge of the system geometry. These existing methods have achieved great success; however, geometry calibration leaves us much room for future improvement.

3 Geometric calibration for different 3-D X-ray imaging systems

The existing methods are suitable for different 3-D X-ray imaging systems, which have a specific scanning trajectory. We will describe the typical methods according to the system where they are employed.

3.1 Calibration for CT

Computed tomography was first introduced in 1971. Since then, it has been widely used in clinical applications. With the development of flat plane detector and computer hardware, it is possible to get a high resolution reconstructed image. In a typical CT system, the image resolution depends on many factors, such as the resolution of the detector, the focal spot size of the X-ray source, the reconstruction method, and the accuracy of the system geometry. In a practical system, the geometry parameters are always inaccurate. This inaccuracy severely impacts the quality of the reconstructed image and makes geometric calibration very necessary [5].

In a typical CT system, such as circular orbit CT or spiral CT, some common parameters should be taken into account [6–8], as shown in Fig. 1:

D: The distance between the X-ray source and the detector

R: The distance between the X-ray source and the rotation center

u_0: The horizontal coordinate of the detector center

v_0: The vertical coordinate of the detector center

φ: The oblique angle of the detector in the horizontal direction

σ: The pitch angle of the detector

η: The oblique angle of the detector in the detector plane

$\Delta\beta$: The angle sampling interval

In order to calculate all the parameters above, some methods, which use well-designed phantoms, were proposed [9–11]. For example, in Cho's method, a specially designed phantom which consists of 24 steel ball bearings in a known structure is used. Twelve ball bearings are spaced evenly at 30° in two plane-parallel circles separated by a given distance along the tube axis. Using the ellipse trajectory of the ball bearings in the detector, he can calibrate all the geometric parameters of a CT system. Although this method can calculate all the parameters, it needs a specially designed phantom, which may be very expensive. Besides, the design deviation will influence the accuracy of the calibration, which makes the method hard to be employed in practical applications.

Most mathematical methods do not calculate all the parameters. They use some point-like markers or feature points without specific arrangement in the space. The only prior knowledge may be the distance between each two markers. We will introduce Yang's method as an example in the following section [12].

Yang's method is based on a number of feature points and can estimate the following five system parameters,

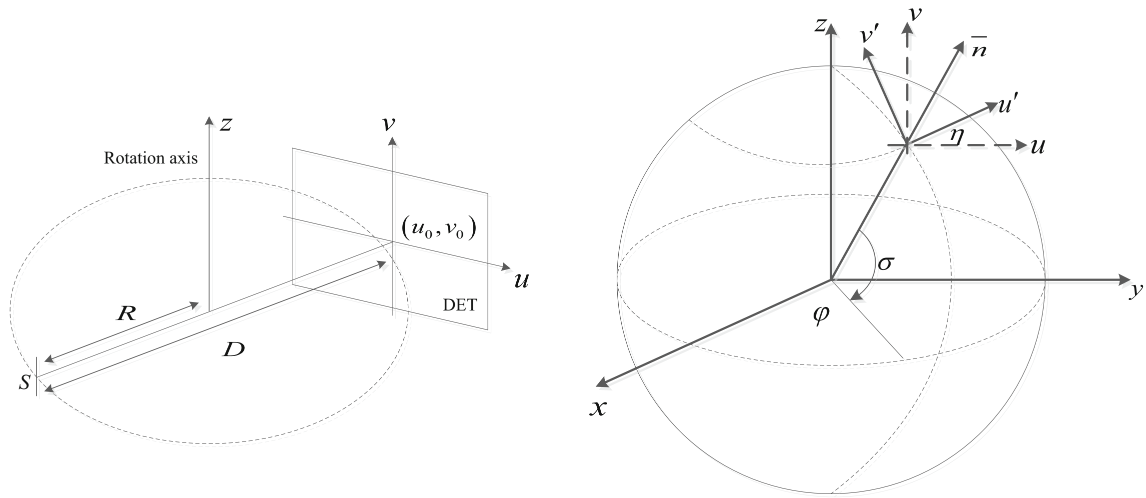

(a) **(b)**

Fig. 1 Geometry parameters of a typical 3-D X-ray imaging system. **a** Definition of the parameters D, R, (u_0, v_0). **b** Definition of the parameters η, σ, φ

D, R, u_0, v_0, and η. For a cone beam CT system, if we assume that only the object rotates and the X-ray tube and detector remain stationary, the orbit of a point in the object during the scan is a circle in a plane parallel to x–y plane. The projection of this circle on the detector plane will be an ellipse. Individual points on this ellipse correspond to the marker's angular positions on the circle. Yang referred to two points on the circular orbit that are exactly 180° out of phase as a radial pair, as shown in Fig. 2a. Thus, the distance, ρ, between a radial pair of points on the detector plane can be calculated. It can be proved that ρ will have the maximum and minimum values when the feature point is on the x axis or y axis for a cone beam CT system with a fan angle less than 60° and a cone angle less than 30°, as shown in Fig. 2b. We can define these feature points as A_{ik} (u_{ik}, v_{ik}), here i refers to the index number of each individual marker, and j is the index number for the four benchmark points on each marker orbit.

Thus, we can calculate the five parameters. For each individual marker, defined

$$X_i = \frac{v_{i1} - v_{i2}}{|A_{i3}A_{i4}|} \quad Y_i = \frac{v_{i1} + v_{i2}}{2}. \tag{1}$$

A linear function $X = a + bY$ can fit all(Y_i, X_i), and we can determine D and v_0,

$$D = b \quad v_0 = a. \tag{2}$$

To calculate η and u_0, when we define the intersection of $A_{i1}A_{i2}$ and $A_{i3}A_{i4}$ as (u_{i0}, v_{i0}), we have

$$u_{i0} = \frac{\begin{vmatrix} \begin{vmatrix} u_{i1} & v_{i1} \\ u_{i2} & v_{i2} \end{vmatrix} & u_{i1} - u_{i2} \\ \begin{vmatrix} u_{i3} & v_{i3} \\ u_{i4} & v_{i4} \end{vmatrix} & u_{i3} - u_{i4} \end{vmatrix}}{\begin{vmatrix} u_{i1} - u_{i2} & v_{i1} - v_{i2} \\ u_{i3} - u_{i4} & v_{i3} - v_{i4} \end{vmatrix}} \quad v_{i0} = \frac{\begin{vmatrix} \begin{vmatrix} u_{i1} & v_{i1} \\ u_{i2} & v_{i2} \end{vmatrix} & v_{i1} - v_{i2} \\ \begin{vmatrix} u_{i3} & v_{i3} \\ u_{i4} & v_{i4} \end{vmatrix} & v_{i3} - v_{i4} \end{vmatrix}}{\begin{vmatrix} u_{i1} - u_{i2} & v_{i1} - v_{i2} \\ u_{i3} - u_{i4} & v_{i3} - v_{i4} \end{vmatrix}}. \tag{3}$$

We found that all (u_{i0}, v_{i0}) can fit the linear function $u_0 = a + bv_0$. After we calculate a and b, we have

$$\eta = \tan^{-1} b. \tag{4}$$

To calculate R, we need the distance l between two markers. Define r_1 and r_2 the two radii of each marker's orbit, as shown in Fig. 3.

We have

$$l^2 = h^2 + r_1^2 + r_2^2 - 2r_1r_2 \cos \alpha. \tag{5}$$

Here

$$h = \frac{|A_{10}A_{20}|}{d}R, \quad r_1 = \frac{|A_{13}A_{14}|}{2d}R, \quad r_2 = \frac{|A_{23}A_{24}|}{2d}R. \tag{6}$$

If we define the original angular position of the two markers as α_{10} and α_{20}, then

$$\alpha_1 = \alpha_{10} - \alpha_{14} \quad \alpha_2 = \alpha_{20} - \alpha_{24} \quad \alpha = \alpha_1 - \alpha_2. \tag{7}$$

Then, we can calculate R

Fig. 2 Calibration geometry of Yang's method. **a** Projection orbit and radial pair. **b** Four benchmark points on each marker orbit [12]

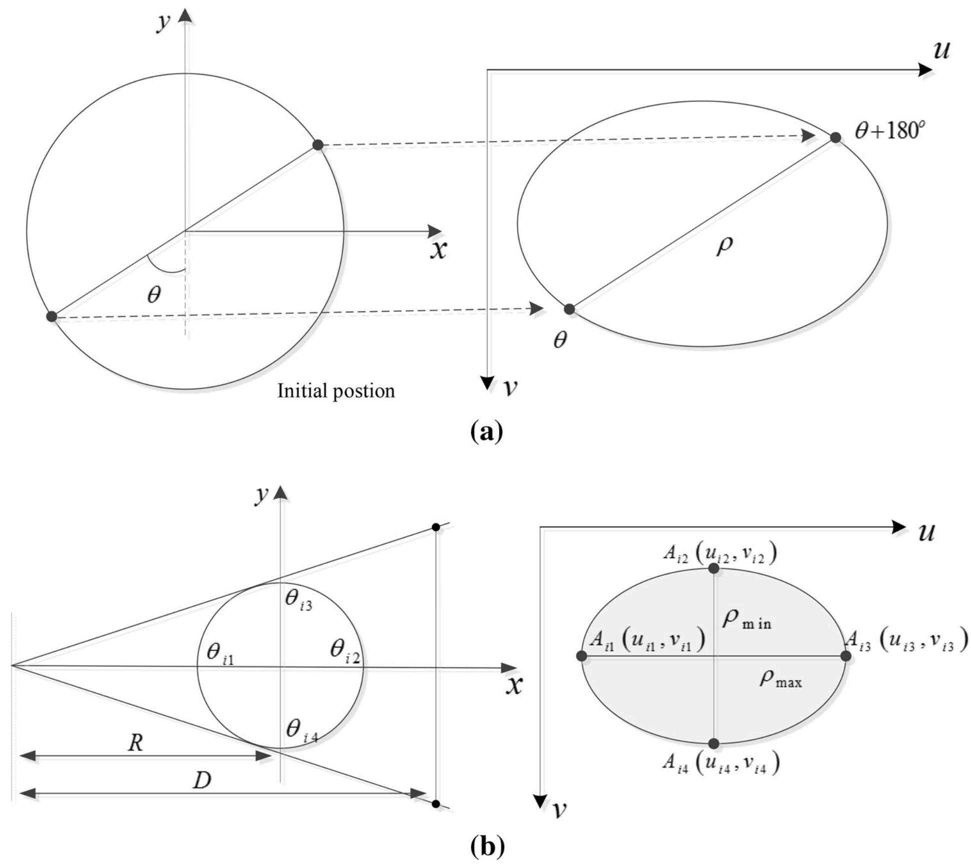

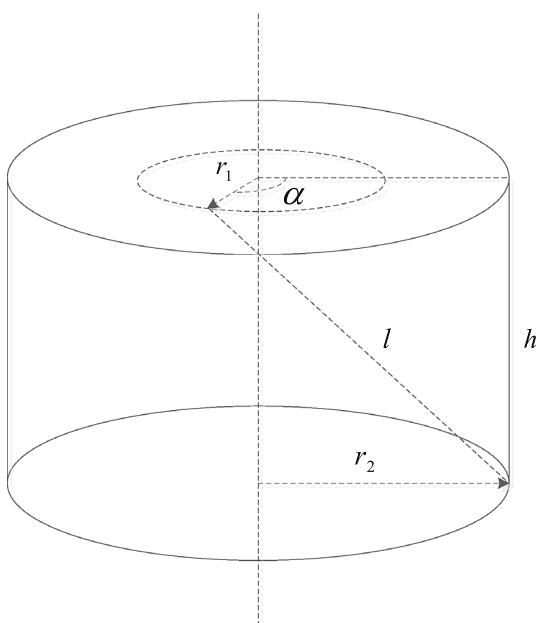

Fig. 3 Distance between two markers in Yang's method

$$R = \frac{l \cdot d}{\sqrt{|A_{10}A_{20}|^2 + \left(\frac{|A_{13}A_{14}|}{2}\right)^2 + \left(\frac{|A_{23}A_{24}|}{2}\right)^2 - \frac{|A_{13}A_{14}| \cdot |A_{23}A_{24}| \cdot \cos\alpha}{2}}}. \tag{8}$$

Then, we have all the five parameters with Yang's method. There are many similar methods, which also calculate part of the system parameters. For example, Noo proposed his analytical method in 2000 and von Smekal proposed a method based on Fourier transform in 2004 [13, 14]. Beque calibrated the geometry using an object with three spheres [15]. The common point of these methods is that they use more than one projection to determine the geometric parameters for each source position. Other methods calculate parameters for each projection separately and independently of all other projections [16–19]. Besides, there are also methods which calibrate the system geometry by estimating a general projection matrix [20]. Due to the space limitations, we will not discuss these methods in detail in this paper.

In conclusion, all these methods are designed for a typical CT system with a circle-plus-arc trajectory and may not be suitable for other imaging systems. Each of them has their own limitations and advantages. Some can give an accurate system geometry and calculate all the geometric parameters with well-designed phantoms. However, the phantoms may be very complicated, precise, and expensive, which make these methods only applicable to experimental research. Other methods are more suitable for practical applications due to their low requirement to the calibration phantoms. However, they can only calculate parts of the system parameters. All these methods can help us to improve the quality of the reconstructed image, and we can choose an appropriate method according to the needs of different applications.

3.2 Calibration for digital X-ray tomosynthesis

Tomosynthesis was first introduced at almost the same time as CT. Due to some technical limitations, it was not widely used until the appearance of flat panel detector [21]. Nowadays, digital X-ray tomosynthesis has become more and more popular in practical applications, especially in clinical applications, such as breast tomosynthesis and dental tomosynthesis [22]. There are three typical scanning modes in a tomosynthesis system, as shown in Fig. 4 [23]. A completely isocentric motion is shown in Fig. 4a. Both the X-ray source and detector rotate around a common axis within the object. Figure 4b is the most classic tomosynthesis scanning method, a partial isocentric motion. The detector moves in a line or a circle within one plane. And the X-ray source rotates around a certain rotation center. In some applications, the detector has to be stationary due to the limited space, as shown in Fig. 4c. Both the object and detector stay still while the X-ray source moves along a trajectory around them, for example, the breast tomosynthesis system.

In a typical tomosynthesis system, the imaged object is fixed in a certain position and the X-ray source assumes different discrete positions along a trajectory in space. For each source position, a projection radiography image is acquired and then sent to the tomosynthesis system. Accurate image reconstruction also requires a precise knowledge of the system geometry. There have been many methods that calibrate the 3-D X-ray tomosynthesis system geometry. However, the tomosynthesis system includes a different geometry for each acquired image, typically because of the change in the X-ray source location for each acquired image. This means that methods may not acquire a satisfying result [24–26].

Many tomosynthesis geometric calibration methods are based on some well-designed phantoms. For example, Wang and Godfrey proposed similar methods, which employ some point-like markers to estimate possible deviation in tomosynthesis geometry and reduce these deviations to get a better reconstructed image [27, 28]. Hui et al. proposed a method using a phantom with ten fiducial markers. With this phantom, the projection matrices of an experimental digital tomosynthesis prototype are acquired from each projection view under a series of misalignment conditions [29]. Although these methods can acquire a relatively accurate system geometry, the phantom used is relatively complex and is not convenient for clinical applications. In 2005, GE (General Electric Company) proposed a method using some fiducial markers with non-determined positions. In GE's method, the geometry is determined by arbitrarily locating at least two markers within the imaged volume and locating the projections of the markers within at least two images corresponding to different positions of a focal spot of the X-ray source. For every X-ray source position, one image acquired must be included in at least two images, as shown in Fig. 5 [30].

P and Q denote two different focal spot positions of the X-ray source, and A and A' denote two different fiducial marker positions. B and B' and C and C' denote the respective locations of the projections of the markers A and A', generated by acquiring a projection image with P and Q. Then, the method calibrates the geometry by first selecting an arbitrary focal spot position, P, and selecting the first marker position, A, as an arbitrary point between

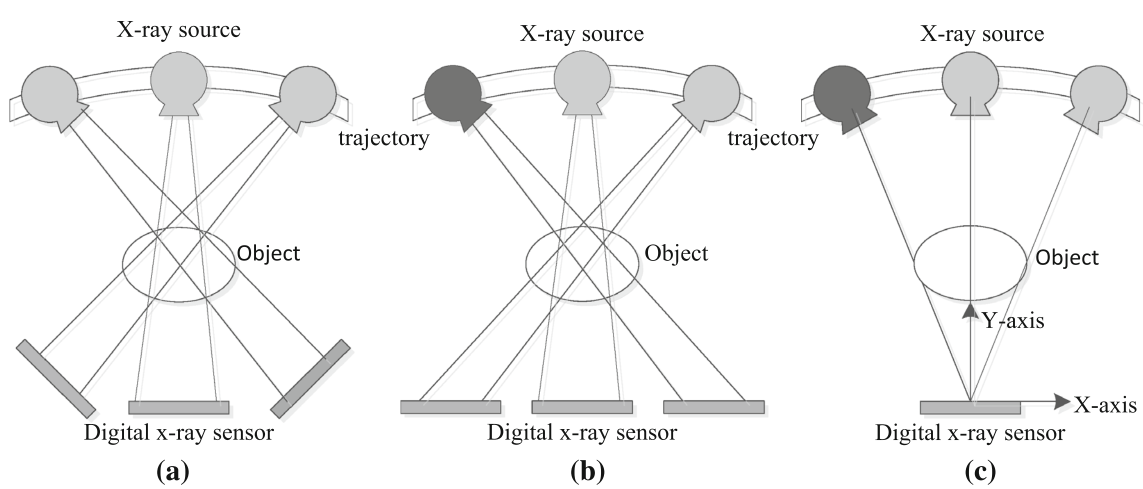

Fig. 4 Three typical digital tomosynthesis scanning mode

P and the corresponding projection, C, located on the line through P and C. Then, the method determines the additional marker, A', as the intersection of the line through A and O with a line through the focal spot, P, and the corresponding projection, C of A'. Then, we can determine the remaining focal spot position, Q, as the intersection of the family of lines. This method can calibrate tomosynthesis geometry using only some fiducial markers with a non-determined position, which is very suitable for practical applications. However, the stability of the method needs to be tested in more experiments.

Generally speaking, these calibration methods for a tomosynthesis system are more tailored, typically because the system has some specific characteristics. The limitations and advantages of each method are similar to those for a CT system. As the development of existing calibration methods is not very consummate, geometry calibration in tomosynthesis leaves us much room for future improvement.

3.3 Calibration for computed laminography (CL)

Laminography techniques are widely used to produce cross-sectional images of selected planes within objects. In some cases, it provides a viable alternative to CT. There are always three scanning types for the CL system: linear, planar, and rotational. Only the rotary bearing movement has a simple geometrical structure, and the space requirement is not as high as the other modes. Furthermore, the beam angle does not need to be as wide as the conventional laminography [31, 32]. We will discuss the rotational scanning mode in the following section as shown in Fig. 6.

The scanning geometry consists of three parts, an X-ray source, a two-dimensional digital flat plane detector, and a rotation gantry. For a practical CL scanning system, the projection of the X-ray focuses on the imaging plane, namely point O, which is not known and cannot be measured by direct means. However, the CL reconstruction algorithm needs the position of the projection of the X-ray focus, so the calibration of the projection coordinate system is the essential step. Barry Eppler introduced a method based on the empirical data gathered during physical calibration and data analytically derived from the empirical data. Other methods may also use some point-like markers to calibrate the system geometry [33]. In 2012, Yang proposed a method using several spherical objects at two geometrical magnification ratio positions in the cone X-ray beam to calibrate the system geometry. We will give a brief introduction of this method in the following section [34].

As shown in Fig. 7, we need to determine the projection of the X-ray focus (point O).

The projection of the point $p_1(x_1, y_1, z_1)$ in the cone beam is point p'_1. When the point p_1 moves to $p_2(x_1, y_1, z_1 + \Delta z)$ with the projection of p'_2 on the imaging plane along the z-axis by a step of Δz, the equation of the lines FP1 and FP2 are:

$$\begin{aligned} \mathrm{FP1}: \frac{x}{x_1} = \frac{y}{y_1} = \frac{z - D}{z_1 - D} \\ \mathrm{FP2}: \frac{x}{x_1} = \frac{y}{y_1} = \frac{z - D}{z_1 + \Delta z - D}. \end{aligned} \tag{9}$$

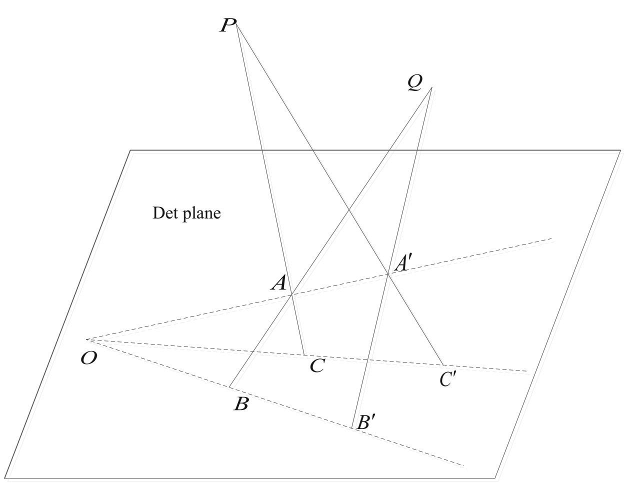

Fig. 5 Principle diagram of GE's calibration method

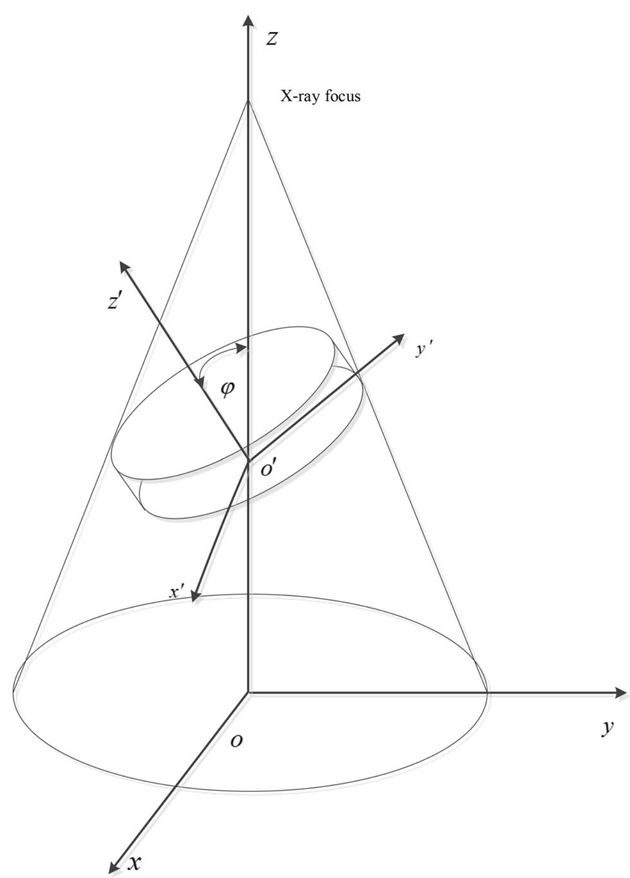

Fig. 6 Principle diagram of cone beam CL scanning

Then, we can derive the coordinates of p_1' and p_2':

$$\begin{aligned} p_1' &\to \left(\frac{-Dx_1}{z_1 - D}, \frac{-Dy_1}{z_1 - D}\right) \\ p_2' &\to \left(\frac{-Dx_1}{z_1 + \Delta z - D}, \frac{-Dy_1}{z_1 + \Delta z - D}\right). \end{aligned} \tag{10}$$

Then, the equation of line $p_1'p_2'$ is

$$p_1'p_2' : y = \frac{y_1}{x_1} x. \tag{11}$$

Obviously, line $p_1'p_2'$ passes through O. Thus, for any point in the cone beam, after moving a distance along the central X-ray, the line connecting its new projection point with its original projection point always passes through the projection point of the X-ray focus. So we can set any two points at position p_1 in the cone beam and get their projections, then move them to position p_2 along the central X-ray and get their new projections. The intersection point of the two lines, which connects the projections of the same point, is the projection of the X-ray focus. Then, we have the calibrated geometry.

As we can see, the geometric calibration for the CL system is different from that of other systems, such as CT and tomosynthesis. However, the essence of the calibration is the same. Thus, we can also learn from these calibration methods and this may help us better design calibration methods for other systems.

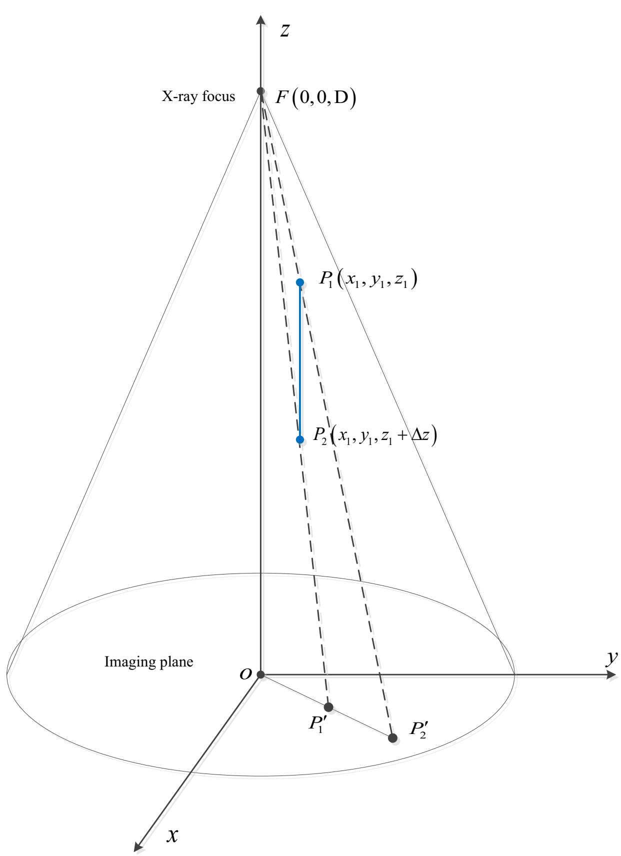

Fig. 7 Principle diagram of calibration method

3.4 Other calibration methods

All the calibration methods discussed above are suitable to some specific imaging modalities. There are some other methods fit for some special imaging modalities, such as linear CT, saddle line CT, and tuned-aperture CT (TACT). As these imaging systems are not widely used in practical applications, calibration methods for these systems are not as well developed as those discussed above.

Due to the relatively special scanning trajectory, calibration methods for those systems always employ several simple markers and determine the system geometry with their locations and projection locations [35]. In 1997, a machine named TACT was introduced for clinical dental diagnosis. TACT is a quais-3-D X-ray imaging technique that may reconstruct the image slices of the region of interest at any depth based on a series of intra-oral radiographs taken from different directions [36]. The principle of TACT is similar to tomosynthesis, and its scanning trajectory is always arbitrary. In order to get an accurate positional relationship between the source and detector, we put some steel or ceramic beads behind the irradiated teeth and took several photos in any source location. Then, we calibrated the geometry with the projection locations of the spheres. However, it is very inconvenient to put markers into a patient's mouth and this makes TACT not used clinically nowadays [37–42].

Although these imaging systems are not widely used in practical applications, the calibration methods for them are worth considering, and we can get valuable reference from them when studying a new calibration method.

4 Numerical simulations

In order to explain the effect of geometric calibration, we chose some typical methods, and some numerical simulations were carried out. The results are shown as follows.

Firstly, we did some simulation with Yang's method in a CT system. The geometry of the system is shown in Fig. 8.

We set the phantom between the source and detector. The size of the sensor is 128×128 mm^2 with 512×512 pixels. The distance, D, between source and detector is 300 mm. The distance between the R source and the coordinate origin is 180 mm. The source, coordinate origin, and the center of the detector plane are located in a straight line. Then, we add some random errors to both D and R. Also we give the detector a micro-offset. After

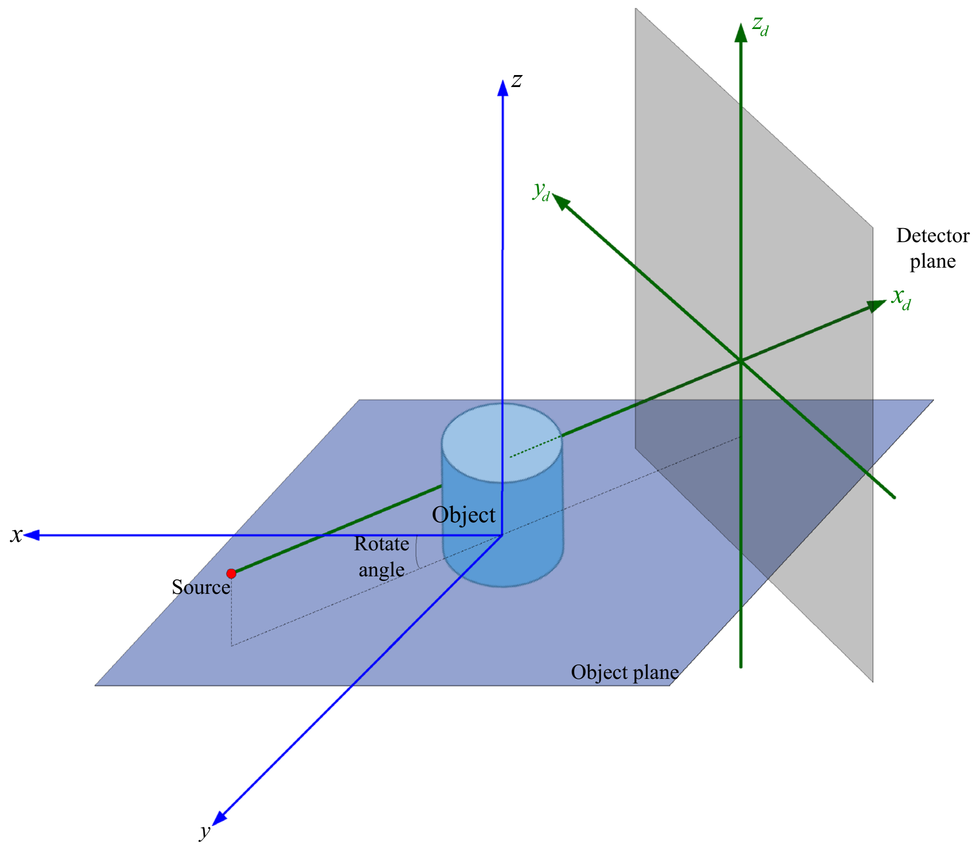

Fig. 8 Geometry of the CT system

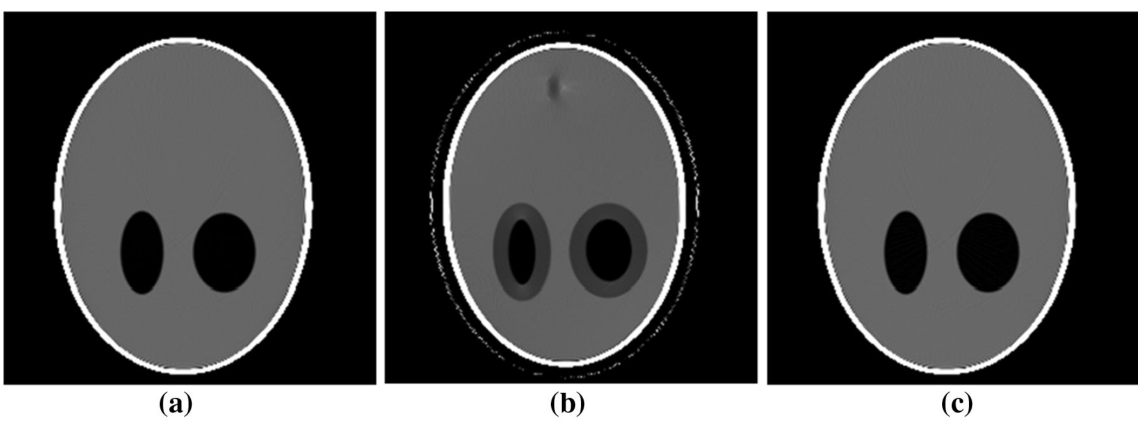

Fig. 9 Center slice of different reconstructed results

that, we get 360 projections from 0 to 360°. And the images are reconstructed using the FDK algorithm with three kinds of system geometry. They are the accurate geometry, the calibrated geometry, and the geometry with random errors. The center slices of different results are shown in Fig. 9.

As shown in Fig. 9, Fig. 9a is the reconstructed image with accurate system geometry, while Fig. 9c is the one that is reconstructed with calibrated geometry. Compared to Fig. 9b, which is reconstructed without geometric calibration, we find that Fig. 9c has a higher contrast in details and can be the one that reconstructed the image with accurate geometry. This explains the effects of the geometric calibration methods.

Also, we carried out a simulation using a tomosynthesis system with GE's method. The simulation geometry is shown in Fig. 10.

We set the distance of the X-ray focal spot to the center of the sensor at 300 mm. The origin of the coordinate was located at the center of the sensor. The detector remained stationary during IDT scanning. The size of the sensor was

20×20 mm^2 with 1000×1000 pixels. The phantom we used was consisted of 27 balls distributed in three layers. The size of the phantom was $10 \times 10 \times 10$ mm^3 with $512 \times 512 \times 512$ pixels, as shown in Fig. 10b. The X-ray source moved with angular ranges of ±30° and an angular interval of 3°. The images were reconstructed on $512 \times 512 \times 512$ grids. The distance between the trajectory and the detector plane is 300 mm. Then, we added some random errors to the 3-D coordinates of each source position. Using these new source positions, we got 21 projections. After that, we reconstructed the image with three kinds of system geometry. The center slices of the different results are shown in Fig. 11.

As shown in Fig. 11, Fig. 11a is the reconstructed image without geometric calibration, Fig. 11b is reconstructed with calibrated geometry, and Fig. 11c is the one that was reconstructed with accurate geometry. As the offsets of our original source positions are limited, the differences between the reconstructed images are not so significant. However, we also found that the reconstructed slice with a calibrated geometry is better than that without geometric calibration.

In a conclusion, we can see from the above simulations that geometric calibration can help us get better reconstructed images. We can easily obtain a high image quality and a high level of detail resolution of the reconstructed structure of the imaged object with calibrated system geometry.

5 Discussion and conclusion

A precise knowledge of geometry is always pivotal to a 3-D X-ray imaging system. We can easily obtain a high image quality and a high level of detail resolution of the reconstructed structure in the imaged object with an

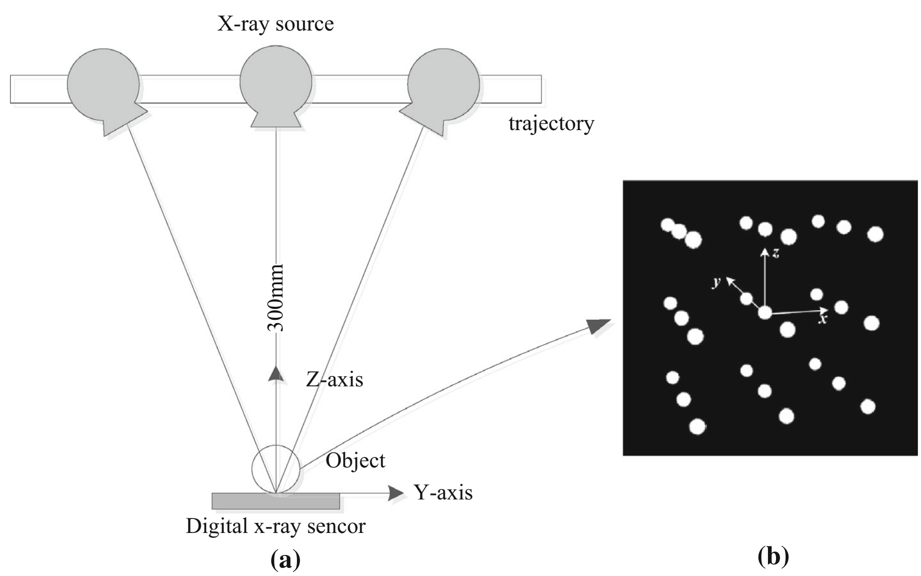

Fig. 10 Simulation using tomosynthesis system

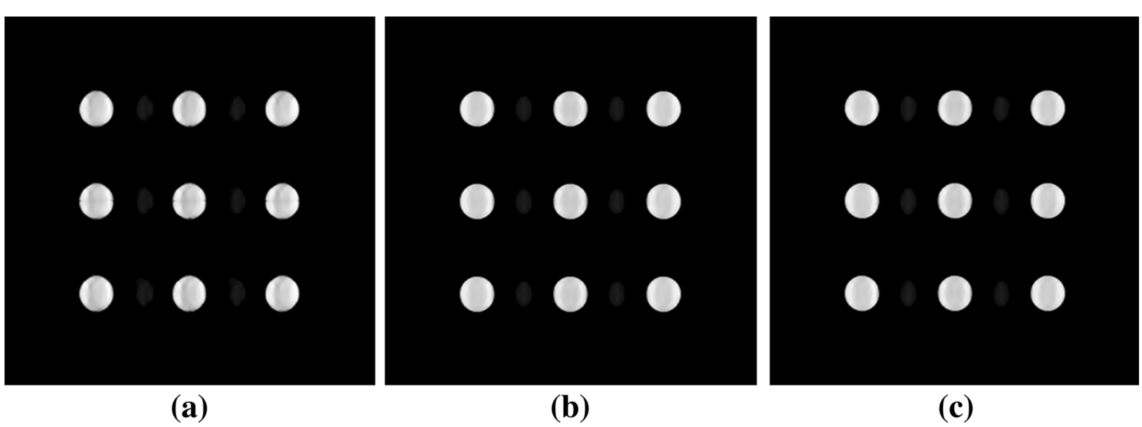

Fig. 11 Center slice of different reconstructed results

accurate system geometry. Various calibration methods have been proposed in order to get a relatively reliable geometry. Most of them use some markers and calculate the system geometry with a mathematical method, such as the analytical method, transform domain method, or iterative approach. These methods are easy to operate when dealing with practical applications. However, they are only suitable for some specific imaging modalities and can only calibrate part of the geometric parameters. Other methods may get a better calibrated geometry, as they use a custom phantom designed according to the imaging system. However, these phantoms are always very complex and expensive. Besides, phantoms need a special design and the design deviation will influence the accuracy of the calibration. All these limitations make them hard to be employed in practical applications. Furthermore, calibration methods, which can be applied to any kind of imaging modalities, also exist, but the accuracy and stability remain a problem to be solved.

Although these existing methods have acquired great achievements, there is much room for improvement in geometric calibration. Future work may focus on methods which can apply to different imaging modalities with fewer markers. Furthermore, we may use some iterative methods to optimize the system geometry when doing image reconstruction; thus, we can eliminate the calibration step.

References

1. L. Li, Z.Q. Chen, Y.X. Xing et al., A general exact method for synthesizing parallel-beam projections from cone-beam projections via filtered backprojection. Phys. Med. Biol. **51**, 5643–5654 (2006). doi:10.1088/0031-9155/51/21/017
2. Z.Q. Chen, X. Jin, L. Li, Ge. Wang, A limited-angle CT reconstruction method based on anisotropic TV minimization. Phys. Med. Biol. **58**, 2119–2141 (2013). doi:10.1088/0031-9155/58/7/2119
3. X. Wang, J.G. Mainprize, M.P. Kempston, et al. Digital breast tomosynthesis geometry calibration//Medical imaging. Int. Soc. Opt. Photonics 65103B (2007). doi:10.1117/12.698714
4. L. Helfen, T. Baumbach, P. Mikulík et al., High-resolution three-dimensional imaging of flat objects by synchrotron-radiation computed laminography. Appl. Phys. Lett. **86**, 071915 (2005). doi:10.1063/1.1854735
5. S. Hoppe, F. Noo, F. Dennerlein et al., Geometric calibration of the circle-plus-arc trajectory. Phys. Med. Biol. **52**, 6943–6960 (2007). doi:10.1088/0031-9155/52/23/012
6. G.T. Gullberg, B.M.W. Tsui, C.R. Crawford et al., Estimation of geometrical parameters for fan beam tomography. Phys. Med. Biol. **32**, 1581–1594 (1987). doi:10.1088/0031-9155/32/12/005
7. G.T. Gullberg, B.M.W. Tsui, C.R. Crawford et al., Estimation of geometrical parameters and collimator evaluation for cone beam tomography. Med. Phys. **17**, 264–272 (1990). doi:10.1118/1.596505
8. L. Li, Z.Q. Chen, L. Zhang, Y.X. Xing, K.J. Kang, A cone-beam tomography system with a reduced size planar detector: a backprojection-filtration reconstruction algorithm as well as numerical and practical experiments. J Appl Radiat Isot. **65**, 1041–1047 (2007). doi:10.1016/j.apradiso.2007.01.023
9. Y. Cho, D.J. Moseley, J.H. Siewerdsen, D.A. Jaffray, Accurate technique for complete geometric calibration of cone-beam computed tomography systems. Med. Phys. **32**, 968–983 (2005). doi:10.1118/1.1869652
10. Y. Sun, Y. Hou, F. Zhao, J. Hu, A calibration method for misaligned scanner geometry in cone-beam computed tomography. NDT E Int. **39**, 499–513 (2006). doi:10.1016/j.ndteint.2006.03.002
11. C. Mennessier, R. Clackdoyle. Automated geometric calibration and reconstruction in circular cone-beam tomography[C]//Nuclear Science Symposium Conference Record, 2008. NSS'08. IEEE. IEEE, 2008: 5081–5085. doi:10.1109/NSSMIC.2008.4774380
12. K. Yang, A.L.C. Kwan, D.F. Miller, J.M. Boone, A geometric calibration method for cone beam CT systems. Med. Phys. **33**, 1695–1706 (2006). doi:10.1118/1.2198187
13. F. Noo, R. Clackdoyle, C. Mennessier, T.A. White, T.J. Roney, Analytic method based on identification of ellipse parameters for scanner calibration in cone-beam tomography. Phys. Med. Biol. **45**, 3489–3508 (2000). doi:10.1088/0031-9155/45/11/327
14. L. von Smekal, M. Kachelrieß, E. Stepina, Willi A. Kalender. Geometric misalignment and calibration in cone-beam tomography. Med. Phys. **31**, 3242–3266 (2004). doi:10.1118/1.1803792
15. D. Beque, J. Nuyts, P. Suetens, G. Bormans, 2005 Optimization of geometrical calibration in pinhole spect. IEEE Trans. Med. Imaging **24**, 180–190 (2005). doi:10.1109/TMI.2004.839367
16. G. Chen, J. Zambelli, B. Nett, M. Supanich et al., Design and development of C-arm based cone-beam CT for image-guided interventions: initial results Proc. SPIE **6142**, 336–347 (2006). doi:10.1117/12.653197
17. G. Strubel, R. Clackdoyle, C. Mennessier, F. Noo, 2005 Analytic calibration of cone-beam scanners. IEEE Nucl. Sci. Symp. Conf. Rec. **5**, 2731–2735 (2005). doi:10.1109/NSSMIC.2005.1596901
18. N.K. Strobel, B. Heigl, T.M. Brunner et al., Improving 3D image quality of x-ray C-arm imaging systems by using properly designed pose determination systems for calibrating the projection geometry[C]//Medical Imaging. Int. Soc. Opt. Photonics **2003**, 943–954 (2003). doi:10.1117/12.479945
19. D. Panetta, N. Belcari, A. Del Guerra et al., An optimization-based method for geometrical calibration in cone-beam CT without dedicated phantoms. Phys. Med. Biol. **53**, 3841–3861 (2008). doi:10.1088/0031-9155/53/14/009
20. A. Ladikos, W. Wein. Geometric calibration using bundle adjustment for cone-beam computed tomography devices[C]//SPIE medical imaging. Int. Soc. Opt. Photonics 83132T (2012). doi:10.1117/12.906238
21. L. Li, Z. Chen, Z. Zhao et al., X-ray digital intra-oral tomosynthesis for quasi-three-dimensional imaging: system, reconstruction algorithm, and experiments. Opt. Eng. **52**, 013201 (2013). doi:10.1117/1.OE.52.1.013201
22. L.T. Niklason, B.T. Christian, L.E. Niklason et al., Digital tomosynthesis in breast imaging. Radiology **205**, 399–406 (1997)
23. J.T. Dobbins III, D.J. Godfrey, Digital x-ray tomosynthesis: current state of the art and clinical potential. Phys. Med. Biol. **48**, R65 (2003). doi:10.1088/0031-9155/48/19/R01
24. P.R. Bakic, P. Ringer, J. Kuo, et al. *Analysis of Geometric Accuracy in Digital Breast Tomosynthesis Reconstruction[M]//Digital Mammography* (Springer, Berlin, 2010), pp. 62–69. doi:10.1007/978-3-642-13666-5_9
25. Z. Kolitsi, G. Panayiotakis, V. Anastassopoulos et al., A multiple projection method for digital tomosynthesis. Med. Phys. **19**, 1045–1050 (1992). doi:10.1118/1.596822
26. Y.J. Roh, K.W. Koh, H. Cho, et al. Calibration of x-ray digital tomosynthesis system including the compensation for image

distortion[C]//Photonics East (ISAM, VVDC, IEMB). Int. Soc. Opt. Photonics 248–259 (1998). doi:10.1117/12.326966

27. X. Wang, J.G. Mainprize, M.P. Kempston, et al. Digital breast tomosynthesis geometry calibration[C]//medical imaging. Int. Soc. Opt. Photonics 65103B (2007). doi:10.1117/12.698714
28. D.J. Godfrey, F.E. Yin, M. Oldham et al., Digital tomosynthesis with an on-board kilovoltage imaging device[J]. Int. J, Radiat. Oncol. **65**, 8–15 (2006). doi:10.1016/j.ijrobp.2006.01.025
29. H. Miao, X. Wu, H. Zhao et al., A phantom-based calibration method for digital x-ray tomosynthesis. J. X-Ray Sci. Technol. **20**, 17–29 (2012). doi:10.3233/XST-2012-0316
30. B. Claus, B. Opsahl-Ong, M. Yavuz. Method, apparatus, and medium for calibration of tomosynthesis system geometry using fiducial markers with non-determined position [P]. 2003-6-25
31. M. Maisl, F. Porsch, C. Schorr. Computed laminography for X-ray inspection of lightweight constructions[C]//2nd International Symposium on NDT in Aerospace. 2010: M0
32. J.M. Que, D.Q. Cao, W. Zhao et al., Computed laminography and reconstruction algorithm. Chin. Phys. C. **36**, 777–783 (2012). doi:10.1088/1674-1137/36/8/017
33. B. Eppler. Method and apparatus for calibrating an x-ray laminography imaging system: U.S. Patent 6,819,739[P]. 2004-11-16
34. M. Yang, J. Zhang, M. Yuan et al., Calibration method of projection coordinate system for X-ray cone-beam laminography scanning system. NDT E Int. **52**, 16–22 (2012). doi:10.1016/j.ndteint.2012.08.005
35. N. Robert, K.N. Watt, X. Wang et al., The geometric calibration of cone–beam systems with arbitrary geometry. Phys. Med. Biol. **54**, 7239–7261 (2009). doi:10.1088/0031-9155/54/24/001
36. R.L. Webber, R.A. Horton, D.A. Tyndall et al., Tuned-aperture computed tomography (TACT^{TM}): theory and application for three-dimensional dento-alveolar imaging. Dentomaxillofac. Radiol. **26**, 53–62 (1997). doi:10.1038/sj.dmfr.4600201
37. K. Yamamoto, A.G. Farman, R.L. Webber et al., Effects of projection geometry and number of projections on accuracy of depth discrimination with tuned-aperture computed tomography (TACT) in dentistry. Oral Surg. Oral Med. Oral Pathol. Oral Radiol. Endod. **86**, 126–130 (1998). doi:10.1016/S1079-2104(98)90162-7
38. R.L. Webber, J.K. Messura, An in vivo comparison of diagnostic information obtained from aperture computed tomography and conventional dental radiographic imaging modalities. Oral Surg. Oral Med. Oral Pathol. Oral Radiol. Endod. **88**, 239–247 (1999). doi:10.1016/S1079-2104(99)70122-8
39. K. Yamamoto, R.L. Webber, R.A. Horton et al., Effect of number of projections on accuracy of depth discrimination using tuned-aperture computed tomography for 3-dimensional dentoalveolar imaging of low-contrast details. Oral Surg. Oral Med. Oral Pathol. Oral Radiol. Endod. **88**, 100–105 (1999). doi:10.1016/S1079-2104(99)70201-5
40. M.K. Nair, U.D.P. Nair, H. Gröndahl et al., Detection of artificially induced vertical radicular fractures using tuned aperture computed tomography. Eur. J. Oral Sci. **109**, 375–379 (2001). doi:10.1034/j.1600-0722.2001.00085.x
41. A.G. Farman, J.P. Scheetz, P.D. Eleazer et al., Tuned-aperture computed tomography accuracy in tomosynthetic assessment for dental procedures. Int. Congr. Ser. **1230**, 695–699 (2001). doi:10.1016/S0531-5131(01)00113-3
42. D.J. Barton, S.J. Clark, P.D. Eleazer et al., Tuned-aperture computed tomography versus parallax analog and digital radiographic images in detecting second mesiobuccal canals in maxillary first molars. Oral Surg. Oral Med. Oral Pathol. Oral Radiol. Endod. **96**, 223–228 (2003). doi:10.1016/S1079-2104(03)00061-1